Published in final edited form as:
J Magn Reson Imaging. 2010 May ; 31(5): 1242–1251. doi:10.1002/jmri.22138.

Quantitative Multi-Parametric PROPELLER MRI of Diethylnitrosamine-Induced Hepatocarcinogenesis in Wister Rat model

Jie Deng, PhD[1,2], **Ning Jin, MS**[1,2], **Xiaoming Yin, MS**[1,2], **Guang-Yu Yang, MD**[3], **Zhuoli Zhang, MD**[1], **Reed A. Omary, MD, MS**[1,2,4], and **Andrew C. Larson, PhD**[1,2,4]

[1]Department of Radiology, Northwestern University

[2]Department of Biomedical Engineering, Northwestern University

[3]Department of Pathology, Northwestern University

[4]Feinberg School of Medicine, Robert H. Lurie Comprehensive Cancer Center, Northwestern University

Abstract

PURPOSE—To develop a quantitative multi-parametric PROPELLER (periodically rotated overlapping parallel lines with enhanced reconstruction) MRI approach and its application in a diethylnitrosamine (DEN) chemically-induced rodent model of hepatocarcinogensis for lesion characterization.

MATERIALS AND METHODS—In nine rabbits with 33 cirrhosis-associated hepatic nodules including regenerative nodule (RN), dysplastic nodule (DN), hepatocellular carcinoma (HCC) and cyst, multi-parametric PROPELLER MRI (diffusion-weighted, T2/M0 (proton density) mapping and T1-weighted) were performed. Apparent diffusion coefficient (ADC) maps, T2 and M0 maps of each tumor were generated. We compared ADC, T2 and M0 measurements for each type of hepatic nodule, confirmed at histopathology.

RESULTS—PROPELLER images and resultant parametric maps were inherently co-registered without image distortion or motion artifacts. All types of hepatic nodules demonstrated complex imaging characteristics within conventional T1- and T2-weighted images. Quantitatively, cysts were distinguished from RN, DN and HCC with significantly higher ADC and T2; however, there was no significant difference of ADC and T2 between HCC, DN and RN. Mean tumor M0 values of HCC were significantly higher than those of DN, RN and cysts.

CONCLUSION—This study exploited quantitative PROPELLER MRI and multi-dimensional analysis approaches in an attempt to differentiate hepatic nodules in the DEN rodent model of hepatocarcinogensis. This method offers great potential for parallel parameterization during non-invasive interrogation of hepatic tissue properties.

Keywords

PROPELLER MRI; multi-parametric; hepatocarcinogensis; hepatic nodules

Please send correspondence and reprint requests to: Andrew C. Larson, Northwestern University, Department of Radiology, 737 N Michigan Ave, Suite 1600, Chicago, IL 60611, Tel: (312) 926-3499 Fax: (312)926-5991, a-larson@northwestern.edu.

INTRODUCTION

The development of hepatocellular carcinoma (HCC) involves a multi-step carcinogenesis process with varying degrees of cellular and structural atypia beginning with a benign regenerative nodule (RN), progressing to a premalignant dysplastic nodule (DN) and finally overt HCC (1–4). While biopsy serves as the conclusive gold-standard for liver lesion characterization, imaging evaluation of these cirrhosis-associated hepatocellular nodules remains critically important for optimal patient management. Following the diagnosis and treatment of HCC, accurate assessment of therapy response is equally critical to permit timely adjustments to selected therapeutic regimens. HCC size measurements are most commonly used to assess therapy response (5,6). However, a noncompliant cirrhotic liver may limit changes in HCC size (7,8) and treated HCC may be replaced by necrosis or hemorrhage. As a result, lesion size may initially remain unchanged or even increase early after response to therapy. These confounding factors, common to both HCC and a wide range of alternative liver tumor etiologies, have led to the development of quantitative, functional imaging methods for lesion staging and assessment of therapy response (9–13).

Compared to ultrasound and CT, MRI provides superior soft tissue contrast for assessment of cirrhotic nodules. However, there remains considerable overlap and variability of imaging characteristics when attempting to use conventional T1- or T2-weighted MRI to characterize hepatic nodules within a cirrhotic background (4,14,15). Contrast enhanced (CE)-MRI is currently an accepted clinical standard for detection and characterization of HCC based on intra-nodular blood supply (3,4). However, precise timing is critical during CE-MRI to acquire arterial and portal phase images and different lesion stages may continue to exhibit similar enhancement patterns.

Recently, diffusion-weighted MRI (DWI) has been used for both the detection of liver tumors (16–18) and characterization of different types of focal hepatic lesions (19–21). Benign liver lesions including cysts and hemangiomas demonstrate increased apparent diffusion coefficient (ADC) values compared to malignant lesions including HCC and metastases (19–21). Quantitative DWI measurements (22) and combined multi-parametric (ADC + T2 + proton density) MRI measurements (23–25) have demonstrated the potential to differentiate intratumoral tissue types as well as characterize therapy response.

Multi-parametric measurements (ADC + T2 + proton density) recently permitted multi-dimensional analyses to improve tissue classification accuracy in a subcutaneous xenograft murine tumor model (23,24). These methods might also be effective for lesion characterization during hepatocarcinogensis or the detection of HCC therapy response. However, during previous multi-parametric tumor imaging studies, tumors were located within flank or hind-limb tissues with limited motion. Abdominal motion artifacts and mis-registration of the parametric maps could lead to significant challenges during quantitative multi-parametric imaging of the liver.

Single-shot techniques such as half-Fourier acquisition single-shot turbo spin-echo (HASTE) and echo-planar imaging (EPI) have been used for DWI and T2 mapping of the abdomen due to their relative insensitivity to motion artifacts with fast image acquisition (26–28). However, magnetization transfer effects and T2-filtering commonly lead to image blurring for HASTE sequences; and EPI suffers from limited spatial resolution and off-resonance distortion (29,30). These limitations can significantly degrade image quality leading to unreliable quantitative measurements. Multi-shot TSE imaging is less sensitive to susceptibility artifacts and offers the potential for improved spatial resolution. However, multi-shot 2DFT-TSE techniques are more sensitive to motion artifacts. Recently developed multi-shot TSE-based PROPELLER (periodically rotated overlapping parallel lines with

enhanced reconstruction) MRI techniques are less sensitive to motion artifacts due to intrinsic properties of segmental phase correction and oversampling of central *k*-space (31). Importantly, PROPELLER-based sequences can be modified to provide both high quality DWI (32–34) and T2-mapping of the abdomen (35) with reduced sensitivity to motion artifacts and geometric distortion. A combined DWI and T2-mapping PROPELLER approach may offer the potential for precise intra-abdominal multi-parametric measurements during hepatocarcinogensis staging or assessment of therapy response.

The purpose of this study was to develop a quantitative multi-parametric PROPELLER MRI approach and demonstrate the application of these methods in a widely used diethylnitrosamine chemically-induced rodent model of hepatocarcinogensis.

MATERIALS AND METHODS

Animal Model

All experiments were approved by our institutional animal care and use committee (IACUC) and were performed in accordance with institutional guidelines. In 9 Wister rats, oral gavage was performed daily using an 18 gauge gavage needle with 5mL/kg dose 0.3% diethylnitrosamine solution (DEN ISOPAC®, Sigma Chemical Co., USA) for 12 weeks. DEN is a carcinogen primarily targeting the liver in rats. DEN induces various benign and malignant liver lesions in rats with a high success rate and a low mortality rate. Daily gavage administration hastened tumor formation.

MRI Measurements

All MRI studies were performed using a 1.5T Magnetom Espree clinical scanner (Siemens Medical Solutions, Erlangen, Germany). Rats (350g – 500g) were anesthetized with Ketamine (120 – 200 mg/kg) and Xylazine (4–6mg/kg). The abdomen of each rat was fixed with adhesive tape to restrict respiratory movement. The sedated rats were placed within a plastic restraining tube (diameter =10cm) during imaging procedures and a pair of carotid surface coils were used for signal reception.

Following initial localization, multi-parametric PROPELLER imaging was performed at identical contiguous axial slice positions covering the entire liver volume (3mm slice thickness). Common parameters for multi-parametric PROPELLER imaging included: FOV = 120×120 mm^2, matrix = 192×192, spatial resolution = 0.6×0.6×3.0 mm^3, BW= 400 Hz/pixel, multi-slice acquisition during free breathing. For the DW component of the multi-parametric scans, motion probing gradients were applied to provide diffusion weightings of b = 0, 500 and 1000 s/mm^2 with TR/TE = 4950/69 ms, echo train length (ETL) = 15, 168 blade segments (21×8, i.e. blade coverage in *k*-space was 800%), number of slices = 24. The scan time was ~14 minutes for each stack of DW images at each b-value. For the T2-mapping component of the multi-parametric scans, the PROPELLER sequence was modified such that each phase encoding line within each blade segment was sequentially acquired at each echo position along the echo train. These phase encoding lines at each echo position were then re-ordered to reconstruct images at each representative TE (35). The slice thickness ratio between refocusing and excitation RF pulses was adjusted to 3:1 to reduce stimulated echo effects. Specific imaging parameters for T2-mapping component were: TR = 4000 ms, TE_i = i × echo spacing (i =1, 2,…,ETL), ETL = 25, echo spacing (ES) =8 ms, 13 blade segments, excitation slice thickness = 3mm, number of slices = 12, slice gap = 100%. Two separate acquisitions with interleaved slice positions were performed to cover all slices. The scan time for T2 mapping was 25 minutes for each stack of slices. Finally, an additional set of T1W PROPELLER images was acquired at all slice positions with TR/TE = 200 / 8 ms, ETL = 9, 170 segments, number of slices = 24.

Histopathologic Evaluation

Each rat was euthanized with intravenous injection of Euthasol at a dose of 150 mg/kg and bilateral thoracotomy. Rat livers were fixed in 10% buffered formaldehyde solution and sliced at 3 mm intervals in the axial plane to correspond to the plane of MR images as closely as possible. Those liver slices with tumor nodules were embedded in paraffin for histological evaluation. These nodules were sectioned into 4μm slices and stained using hematoxylin and eosin (H&E). H&E cell staining and cell morphology were characterized by an attending surgical pathologist with specialization in gastrointestinal oncology (>10 years experience). Using the diagnostic criteria from the International Working Party's "Terminology of Nodular Hepatocellular Lesions" (2), nodules were classified as cyst, RN, DN or HCC. H&E slides were digitized with optical magnification (×400) using a multispectral imaging system (Nuance, CRI, Woburn, MA).

Image Analysis

Image post-processing was performed offline using Matlab software (MathWorks, Natick, MA). ADC parametric maps were reconstructed from each set of DW images at each slice position. ADC values of each pixel were calculated as the slope of the least-squares fitting line to the function: $\mathrm{ADC} \cdot b = \log(S(b) / S(0))$, with $S(b)$ signifying the voxel signal intensity in the image with diffusion weighting of b. Next, T2 parametric maps at each slice position were reconstructed from the TE images with TE = 8 ×{1,3,6,9,12,15,17,20,25}ms. T2 and proton density (M0) values for each pixel were derived by employing the non-linear Levenberg-Marquardt algorithm to fit the mono-exponential function $S(\mathrm{TE_i}) = \mathrm{M0} \cdot \exp(-\mathrm{TE_i} / \mathrm{T2})$.

Lesion ROIs were manually selected upon either diffusion weighted images (b = 0, 500 and 1000 s/mm^2), T2 maps or M0 maps, depending upon the visual conspicuity and delineation of the tumor within these images. Tumor ROIs were then transferred to the corresponding ADC, T2 and M0 maps. Mean ADC, T2 and M0 values over each tumor ROI formed a 3D feature vector. For a total of N tumors, a feature matrix $\mathbf{M}_{N\times 3}$ served as the input for multi-dimensional analysis using the K-means (KM) clustering algorithm. KM clustering is an unsupervised segmentation method without prior knowledge of training data. KM partitions the points in data matrix $\mathbf{M}_{N\times 3}$ into k clusters by iteratively minimizing the sum of point-to-cluster-centroid distances over all clusters. Prior to KM, feature values were normalized with a mean of zero and unit standard deviation. The KM clustering method with k = 4 was initially performed to classify all tumor ROIs into four assumed classes (i.e. cyst, RN, DN and HCC). In addition, we evaluated the use of different KM clustering scenarios by increasing the number of classes (k = 5 and 6) and combining the overlapping classes.

Statistical Analysis

Each set of mean ADC, T2 and M0 measurements were separately compared between cysts, RN, DN and HCC (confirmed at histopathology). An independent pair two-tailed t test with $\alpha = 0.05$ was used for statistical comparisons. Additionally, box-and-whisker plots of the distribution of ADC, T2 and M0 measurements were generated for each type of hepatic nodule.

RESULTS

In a total of 9 rats, 33 cirrhosis-associated hepatic nodules including 17 HCC, 7 RN, 4 DN and 5 cysts were identified at histopathology.

Within PROPELLER images and resultant parametric maps (ADC, T2 and M0 maps), tumor areas were clearly delineated with no motion artifacts or image distortion observed.

Scaled T2 and M0 maps overlaid on corresponding ADC map demonstrated no clearly apparent misregistration between these parametric maps (Fig. 1–3 H, I). Generally, all types of hepatic nodules demonstrated complex imaging characteristics within T1W and T2W images. RN were generally hypo/iso-intense on T2W DW-PROPELLER (b=0 s/mm^2) images but demonstrated variable signal levels on T1W-PROPELLER images. DN signal intensity was highly variable within both T2W and T1W-PROPELLER images. HCC nodules demonstrated variable signal levels compared to surrounding liver tissues on T1W images. HCC at different stages had different signal characteristics within T2W images: smaller HCC tended to be iso-/slightly hyper-intense, whereas larger HCC with intra-tumoral heterogeneity demonstrated mosaic signal intensity patterns.

Representative examples of DW-PROPELLER images with corresponding ADC map, PROPELLER T2 and M0 maps and T1W-PROPELLER image of each liver slice with different types of hepatic nodules are shown in Fig. 1–3. Three larger nodules (maximal diameter = 1.0, 1.7 and 1.6 cm, respectively) characterized as HCC at histopathology are shown in Fig. 1. These HCC tumors were slightly hyper-intense in T2W DW-PROPELLER image (b=0 s/mm^2) (Fig. 1A). With increasing diffusion weighting, HCC demonstrated less signal suppression than surrounding liver tissues (Fig. 1B and 1C). On the corresponding ADC map (Fig. 1D), HCC demonstrated relatively lower ADC values at the viable tumor periphery, likely due to restricted diffusion; necrotic tumor tissues, primarily within the central regions of two HCC tumors, resulted in elevated ADC values compared to peripheral viable tissues. On the T2 map (Fig. 1E), these HCC tumors demonstrated similar or slightly higher T2 values compared to surrounding cirrhotic liver tissues. On the M0 map (Fig. 1F), HCC demonstrated comparable signal intensity with surrounding cirrhotic liver tissues. On the T1W image (Fig. 1G), two HCC were iso-intense but the other one was slightly hypo-intense. Qualitatively, tumor areas depicted in MR images were well correlated to the liver specimen slices at necropsy (Fig. 1J). The magnified H&E images (×400) of tissues within these three nodules were characterized as HCC (Fig. 1K–M).

Fig. 2 demonstrates four nodules within a second animal. Two were characterized as HCC (Fig. 2K and 2L), one as a RN (Fig. 2M) and one as a cyst (Fig. 2N) at histopathology. The cyst had larger ADC (Fig. 2D) and T2 values (Fig .2E) and lower M0 values (Fig. 2F), but was hypo-intense on T1W image (Fig. 2G) compared to surrounding tissues and the other three nodules. On DW-PROPELLER images (b = 500 s/mm^2 and 1000 s/mm^2)(Fig. 2B and 2C), both HCC demonstrated less signal suppression compared to the RN, therefore resulting in lower ADC values for these lesions within the corresponding ADC map (ADC_{HCC} = 1.7 and 1.5 ×10^{-3} mm^2/s, ADC_{RN} = 2.4 ×10^{-3} mm^2/s) (Fig. 2D). The two HCC were slightly hyper-intense than the RN on T2W PROPELLER image (b=0s/mm^2) (Fig. 2A). Quantitatively, the two HCC ($T2_{HCC}$ = 89.4 and 83.8 ms) and RN ($T2_{RN}$ = 77.7ms) had lower T2 values compared to the cyst ($T2_{cyst}$ = 1558 ms); while the RN had slightly lower T2 value compared to two HCC. However, these two HCC demonstrated variable signal characteristics on M0 map (Fig. 2F) and T1W image (Fig. 2G): the right-side larger HCC was hypo-intense and the left-side smaller HCC was hyper-intense on both M0 map and T1W image. Qualitatively, tumor areas depicted in MR images were well correlated with tumor positions within the liver specimen slice at necropsy (Fig. 2J).

Fig. 3 shows three hepatic nodules within a third animal. Two lesions were characterized as RN (Fig. 3K and 3L) and one as a DN (Fig. 3M) at histopathology. On the T2 map (Fig. 3E), both RNs had slightly higher T2 values ($T2_{RN}$ = 77.7 and 80 ms) compared to surrounding cirrhotic liver tissues; while DN demonstrated even higher T2 values ($T2_{DN}$ = 134.5 ms). On the ADC map (Fig. 3D), both RNs demonstrated lower ADC values (ADC_{RN} = 1.1 and 2.1×10^{-3} mm^2/s) compared to the DN (ADC_{DN} = 3.7×10^{-3} mm^2/s). On the M0 map (Fig. 3F) and T1W image (Fig. 3G), DN and the smaller RN were not differentiated

from the surrounding liver tissues; however, the larger RN was hyper-intense compared to the surrounding liver tissues on both M0 map and T1W image.

Box-and-Whisker plots of tumor ADC, T2 and M0 values for each type of hepatic nodule are shown in Fig. 4. Mean ADC values for HCC, DN, RN and cysts were 1.84±0.36 $\times 10^{-3}$ mm^2/s, 2.2±0.92 $\times 10^{-3}$ mm^2/s, 1.7±0.45 $\times 10^{-3}$ mm^2/s and 4.0±0.30 $\times 10^{-3}$ mm^2/s, respectively. ADC values of cysts were significantly higher than those of HCC, DN and RN ($p < 0.05$); however, there was no significant difference of ADC values between HCC, DN and RN. Mean T2 values for HCC, DN, RN and cysts were 115.8±86.2 ms, 87.6±20.5 ms, 77.2±15.1ms and 1455±326.4ms, respectively. Similar to the ADC measurements, T2 values of cysts were significantly higher than those of the other three types ($p < 0.05$); however, there was no significant difference of T2 values between HCC, DN and RN. In contrast, mean tumor M0 values of HCC (702.4±173, arbitrary unit) were significantly higher than those of DN (514.5±53.8), RN (505.4±183.6) and cysts (370.5±113); however, no significant difference of M0 values was observed between DN, RN and cysts.

Using KM clustering method (k = 4), all the nodules were classified into four categories (I −IV) (Table 1). All cysts (n = 5) were classified in category IV, clearly differentiated from other three types of hepatic nodules with much higher ADC and T2 values and lower M0 values. There was considerable overlap between HCC, DN and RN classification in categories II and III. However, HCC in category I was uniquely distinguished from the other nodules. ADC values of HCC in category I were 1.4 ± 0.19 $\times 10^{-3}$ mm^2/s, lower than those of HCC in category II (2.0 ± 0.35 $\times 10^{-3}$ mm^2/s) and category III (1.9 ± 0.1 $\times 10^{-3}$ mm^2/s); T2 values of HCC in category I were 93.6 ± 9.7ms, similar to those of HCC in category III (82.1 ± 2.5ms) but lower than those of HCC in category II (134.9 ± 110.3ms); M0 values of HCC in category I were 943.4 ± 105.5, higher than those of HCC in category II (680.3 ± 35.7) and category III (454.8 ± 80.5). Using KM clustering with k = 5, HCC, DN and RN still had overlapping distributions in two combined categories (II and III'). Clustering with k = 6 slightly improved the accuracy of nodule classification with HCC (categories I and II) better separated from DN (category III') but with minor overlapping with RN (category II); however, overlapping still existed between HCC, DN and RN in category III'.

DISCUSSION

In this preclinical study, we demonstrated the feasibility of using PROPELLER techniques for multi-parametric quantitative MRI of hepatic nodules in the diethylnitrosamine chemically-induced rodent model of hepatocarcinogensis. The acquired multi-parametric maps (ADC, T2 and M0) were inherently co-registered permitting parallel parameterization for non-invasive interrogation of hepatic tissue properties.

Multi-shot PROPELLER MRI is a promising method for quantitative abdominal oncologic imaging. With the TSE-based acquisition strategy, PROPELLER imaging is less sensitive to susceptibility artifacts and anatomic distortion. It also offers the potential for high spatial resolution with less motion artifacts due to its intrinsic properties of segmental phase corrections and over-sampling of the central *k*-space. A previous study in VX2 liver tumor model (36) demonstrated that DW-PROPELLER imaging and resultant parametric ADC measurements can generate spatially-resolved intra-tumoral viability maps, well correlated with the distribution of viable/necrotic tumor tissues at histopathology. Given these salient properties, DW-PROPELLER and PROPELLER T2 mapping techniques offer the potential to provide inherently co-registered functional parametric maps which may permit more accurate lesion classification and/or characterization of tissue response following either liver directed or systemic therapies.

The development of HCC involves a multi-step pathway beginning with benign regenerative nodules and pre-malignant dysplastic nodules progressing to overtly malignant HCC. Histologically, RN form in response to local proliferation of hepatocytes surrounded by fibrous septa; DN are regenerative nodules containing atypical cells without definitive features of malignance. HCC are a malignant neoplasms composed of cells with hepatocellular differentiation (14). Along the hepatocarcinogenesis pathway, cellular structures become increasingly disorganized and the cellular density increases. Accurate differentiation between cirrhotic nodules can be challenging clinically. Previous studies reported variable signal intensity characteristics of HCC, DN and RN in non-contrast T1W, T2W and DW images (4,14,15). The variable appearance of these cirrhotic nodules could be attributed to the considerable overlap in histopathologic features. Additionally, the visual interpretation of signal intensities could be biased with variable selection of imaging parameters including TR, TE, *b*-values, etc. Our present study qualitatively described very similar observations to those described in previous studies using conventional anatomic MR images (4,14,15). Quantitative measurements of T1, T2 relaxation times, proton density M0 and tissue water mobility may provide more accurate tissue characterization. Xu et al. reported the first use of DWI techniques in evaluating the hepatic nodules including RN, DN and HCC in the DEN rat model (37); this study demonstrated a significant overlap of ADC values between DN, RN and well differentiated HCC, suggesting that the tissue water mobility measurements alone may not be sufficient for tissue characterization. Additionally, these previous studies in the DEN rat model offered relatively limited image quality due to anatomic distortion present in the DW-EPI images and ADC maps. It has been demonstrated that relaxation times are related to the histological differentiation in different types of hepatic tumors and other hepatocellular diseases (38–40), however, they have not been used in differentiation of cirrhosis-associated hepatic nodules during hepatocarcinogensis.

Quantitative multi-dimensional analysis combining ADC, T2, and M0 measurements have recently been investigated in subcutaneous xenograft murine tumor models for voxel-based intra-tumoral tissue heterogeneity (viable tumor, necrosis) and tumor viability measurements (23,24). Our study exploited the multi-dimensional analysis approach in an attempt to differentiate liver lesion types during the hepatocarcinogenesis process. In contrast to the voxel-based classification, our classification approaches were based on the averaged imaging features within tumor ROIs. Of all hepatic nodules including cysts, RN, DN and HCC, cysts were most clearly differentiated from other types of lesions with significantly higher ADC and T2 values. HCC tumors were widely distributed in categorys I, II and III. However, HCC in category I with lower ADC, T2 and higher M0 values were distinguished from those in II and III, possibly attributable to higher cellular density. HCC in category II and III were larger in size with central necrosis and hemorrhage, resulting in increased extracellular water and thus increased tissue water mobility. Intra-tumoral heterogeneity in category II and III HCC may complicate differentiation from DN and RN. Generally, the relatively wider distribution of HCC (among the categories) is likely result from variable nodule size, stage and the histological make-up (15). The lack of lesion differentiation in category II and III could also be due to the rapid progress of hepatocarcinogensis in this model which generates a continuous spectrum of etiologies with overlapping lesion characteristics (37).

There were several limitations in this study. First, the sample size of DN was small. During the fast progression of hepatocarcinogensis in this model, most of the DNs had progressed to HCC or were in late stages during transition to HCC. Further studies with a larger sample size may be necessary to provide a more balanced range of representative hepatic nodules for a more comprehensive analysis. Secondly, our current tumor ROI-based classification method, which neglected intra-tumoral heterogeneity, may account for the low accuracy of lesion type differentiation. In future studies, intra-tumoral voxel-based classification with a

larger number of tissue types and alternative clustering approaches (hierarchical clustering or supervised approaches) may need to be investigated to improve the classification accuracy. A third limitation of this study was the lack of comparisons to dynamic contrast enhanced (DCE) MRI, which may permit the characterization of lesions based upon arterial/portal blood supply and additional tissue perfusion properties. Future studies integrating DCE measurements into the currently proposed multi-parametric analysis may improve the accuracy of tissue characterization during hepatocarcinogensis. Lastly, the scan time was long for DW-PROPELLER and PROPELLER T2 mapping in these rats because of the relatively high resolution (0.6×0.6 mm^2) desired for these studies. Imaging was performed using a clinical scanner without dedicated small animal receiver coils; therefore, multiple signal averages were necessary for adequate SNR. In future translational patient studies, imaging time could be shortened by decreasing the spatial resolution and signal averages, limiting spatial coverage in tumor areas and using parallel imaging techniques. PROPELLER T2 mapping can also be accelerated by using partial echo reordering (35) without adverse impacts on T2 measurement accuracy.

In conclusion, quantitative ADC, T2 and M0 measurements using PROPELLER MRI techniques provided inherently co-registered parametric maps without image distortion or obvious motion artifacts. These functional measurements offer great potential for multidimensional hepatic tissue characterization. Future translational studies should evaluate the use of these multi-dimensional quantitative PROPELLER techniques for clinical lesion staging and assessment of liver tumor therapy response.

Acknowledgments

This work was supported by grant number CA134719 from the NIH National Cancer Institute.

This research is supported by funds from NIH NCI RO1CA134719.

References

1. Coleman WB. Mechanisms of human hepatocarcinogenesis. Curr Mol Med. 2003; 3(6):573–588. [PubMed: 14527088]
2. Terminology of nodular hepatocellular lesions. International Working Party. Hepatology. 1995; 22(3):983–993. [PubMed: 7657307]
3. Efremidis SC, Hytiroglou P. The multistep process of hepatocarcinogenesis in cirrhosis with imaging correlation. Eur Radiol. 2002; 12(4):753–764. [PubMed: 11960222]
4. Hanna RF, Aguirre DA, Kased N, Emery SC, Peterson MR, Sirlin CB. Cirrhosis-associated hepatocellular nodules: correlation of histopathologic and MR imaging features. Radiographics. 2008; 28(3):747–769. [PubMed: 18480482]
5. Miller AB, Hoogstraten B, Staquet M, Winkler A. Reporting results of cancer treatment. Cancer. 1981; 47(1):207–214. [PubMed: 7459811]
6. Therasse P, Arbuck SG, Eisenhauer EA, et al. New guidelines to evaluate the response to treatment in solid tumors. European Organization for Research and Treatment of Cancer, National Cancer Institute of the United States, National Cancer Institute of Canada. J Natl Cancer Inst. 2000; 92(3): 205–216. [PubMed: 10655437]
7. Nauta RJ, Heres EK, Thomas DS, et al. Intraoperative single-dose radiotherapy. Observations on staging and interstitial treatment of unresectable liver metastases. Arch Surg. 1987; 122(12):1392–1395. [PubMed: 3689115]
8. Carr BI. Hepatocellular carcinoma: current management and future trends. Gastroenterology. 2004; 127(5 Suppl 1):S218–S224. [PubMed: 15508087]
9. Kamel IR, Bluemke DA, Eng J, et al. The Role of Functional MR Imaging in the Assessment of Tumor Response after Chemoembolization in Patients with Hepatocellular Carcinoma. J Vasc Interv Radiol. 2006; 17(3):505–512. [PubMed: 16567675]

10. Kamel IR, Bluemke DA, Ramsey D, et al. Role of diffusion-weighted imaging in estimating tumor necrosis after chemoembolization of hepatocellular carcinoma. AJR Am J Roentgenol. 2003; 181(3):708–710. [PubMed: 12933464]
11. Kamel IR, Reyes DK, Liapi E, Bluemke DA, Geschwind JF. Functional MR imaging assessment of tumor response after 90Y microsphere treatment in patients with unresectable hepatocellular carcinoma. J Vasc Interv Radiol. 2007; 18(1 Pt 1):49–56. [PubMed: 17296704]
12. Deng J, Miller FH, Rhee TK, et al. Diffusion-weighted MR imaging for determination of hepatocellular carcinoma response to yttrium-90 radioembolization. J Vasc Interv Radiol. 2006; 17(7):1195–1200. [PubMed: 16868174]
13. Rhee TK, Naik NK, Deng J, et al. Tumor response after yttrium-90 radioembolization for hepatocellular carcinoma: comparison of diffusion-weighted functional MR imaging with anatomic MR imaging. J Vasc Interv Radiol. 2008; 19(8):1180–1186. [PubMed: 18656011]
14. Taouli B, Losada M, Holland A, Krinsky G. Magnetic resonance imaging of hepatocellular carcinoma. Gastroenterology. 2004; 127(5 Suppl 1):S144–S152. [PubMed: 15508078]
15. Silva AC, Evans JM, McCullough AE, Fatoi MA, Vargas HE, Hara AK. MR Imaging of Hypervascular Liver Masses: A Review of Current Techniques. RadioGraphics. 2009; 29:385–402. [PubMed: 19325055]
16. Sandberg, A.; Parikh, T.; Johnson, G.; Stemmer, A.; Xu, J.; Taouli, B. Feasibility of a respiratory-triggered SSEPI diffusion-weighted sequence for liver imaging using navigator echo technique: comparison with breath-hold diffusion-weighted sequence. Proceeding of the 14th Annual Meeting of ISMRM; Seattle. 2006. (Abstract# 400)
17. Coenegrachts K, Delanote J, Ter Beek L, et al. Improved focal liver lesion detection: comparison of single-shot diffusion-weighted echoplanar and single-shot T2 weighted turbo spin echo techniques. Br J Radiol. 2007; 80(955):524–531. [PubMed: 17510250]
18. Zech CJ, Herrmann KA, Dietrich O, Horger W, Reiser MF, Schoenberg SO. Black-blood diffusion-weighted EPI acquisition of the liver with parallel imaging: comparison with a standard T2-weighted sequence for detection of focal liver lesions. Invest Radiol. 2008; 43(4):261–266. [PubMed: 18340250]
19. Namimoto T, Yamashita Y, Sumi S, Tang Y, Takahashi M. Focal liver masses: characterization with diffusion-weighted echo-planar MR imaging. Radiology. 1997; 204(3):739–744. [PubMed: 9280252]
20. Moteki T, Horikoshi H. Evaluation of hepatic lesions and hepatic parenchyma using diffusion-weighted echo-planar MR with three values of gradient b-factor. J Magn Reson Imaging. 2006; 24(3):637–645. [PubMed: 16888790]
21. Bruegel M, Holzapfel K, Gaa J, et al. Characterization of focal liver lesions by ADC measurements using a respiratory triggered diffusion-weighted single-shot echo-planar MR imaging technique. Eur Radiol. 2008; 18(3):477–485. [PubMed: 17960390]
22. Deng J, Rhee TK, Sato KT, et al. In vivo diffusion-weighted imaging of liver tumor necrosis in the VX2 rabbit model at 1.5 Tesla. Invest Radiol. 2006; 41(4):410–414. [PubMed: 16523024]
23. Henning EC, Azuma C, Sotak CH, Helmer KG. Multispectral quantification of tissue types in a RIF-1 tumor model with histological validation. Part I. Magn Reson Med. 2007; 57(3):501–512. [PubMed: 17326181]
24. Carano RA, Ross AL, Ross J, et al. Quantification of tumor tissue populations by multispectral analysis. Magn Reson Med. 2004; 51(3):542–551. [PubMed: 15004796]
25. Henning EC, Azuma C, Sotak CH, Helmer KG. Multispectral tissue characterization in a RIF-1 tumor model: monitoring the ADC and T2 responses to single-dose radiotherapy. Part II. Magn Reson Med. 2007; 57(3):513–519. [PubMed: 17326182]
26. Goldberg MA, Hahn PF, Saini S, et al. Value of T1 and T2 relaxation times from echoplanar MR imaging in the characterization of focal hepatic lesions. AJR Am J Roentgenol. 1993; 160(5): 1011–1017. [PubMed: 8470568]
27. Abe Y, Yamashita Y, Tang Y, Namimoto T, Takahashi M. Calculation of T2 relaxation time from ultrafast single shot sequences for differentiation of liver tumors: comparison of echo-planar, HASTE, and spin-echo sequences. Radiat Med. 2000; 18(1):7–14. [PubMed: 10852650]

28. de Bazelaire CM, Duhamel GD, Rofsky NM, Alsop DC. MR imaging relaxation times of abdominal and pelvic tissues measured in vivo at 3.0 T: preliminary results. Radiology. 2004; 230(3):652–659. [PubMed: 14990831]
29. Constable RT, Gore JC. The loss of small objects in variable TE imaging: implications for FSE, RARE, and EPI. Magn Reson Med. 1992; 28(1):9–24. [PubMed: 1435225]
30. Farzaneh F, Riederer SJ, Pelc NJ. Analysis of T2 limitations and off-resonance effects on spatial resolution and artifacts in echo-planar imaging. Magn Reson Med. 1990; 14(1):123–139. [PubMed: 2352469]
31. Pipe JG. Motion correction with PROPELLER MRI: application to head motion and free-breathing cardiac imaging. Magn Reson Med. 1999; 42(5):963–969. [PubMed: 10542356]
32. Deng J, Miller FH, Salem R, Omary RA, Larson AC. Multishot diffusion-weighted PROPELLER magnetic resonance imaging of the abdomen. Invest Radiol. 2006; 41(10):769–775. [PubMed: 16971801]
33. Deng J, Omary RA, Larson AC. Multishot diffusion-weighted SPLICE PROPELLER MRI of the abdomen. Magn Reson Med. 2008; 59(5):947–953. [PubMed: 18429036]
34. Pipe JG, Farthing VG, Forbes KP. Multishot diffusion-weighted FSE using PROPELLER MRI. Magn Reson Med. 2002; 47(1):42–52. [PubMed: 11754441]
35. Deng J, Larson AC. Modified PROPELLER Approach for T2-Mapping of the Abdomen. Magn Reson Med. 2009; 61(6):1269–1278. [PubMed: 19353672]
36. Deng J, Virmani S, Young J, et al. Diffusion-weighted PROPELLER MRI for quantitative assessment of liver tumor necrotic fraction and viable tumor volume in VX2 rabbits. J Magn Reson Imaging. 2008; 27(5):1069–1076. [PubMed: 18407540]
37. Xu H, Li X, Xie JX, Yang ZH, Wang B. Diffusion-weighted magnetic resonance imaging of focal hepatic nodules in an experimental hepatocellular carcinoma rat model. Acad Radiol. 2007; 14(3): 279–286. [PubMed: 17307660]
38. Farraher SW, Jara H, Chang KJ, Ozonoff A, Soto JA. Differentiation of hepatocellular carcinoma and hepatic metastasis from cysts and hemangiomas with calculated T2 relaxation times and the T1/T2 relaxation times ratio. J Magn Reson Imaging. 2006; 24(6):1333–1341. [PubMed: 17083093]
39. Cittadini G, Santacroce E, Giasotto V, Rescinito G. Focal liver lesions: characterization with quantitative analysis of T2 relaxation time in TSE sequence with double echo time. Radiol Med. 2004; 107(3):166–173. [PubMed: 15031682]
40. Cieszanowski A, Szeszkowski W, Golebiowski M, Bielecki DK, Grodzicki M, Pruszynski B. Discrimination of benign from malignant hepatic lesions based on their T2-relaxation times calculated from moderately T2-weighted turbo SE sequence. Eur Radiol. 2002; 12(9):2273–2279. [PubMed: 12195480]

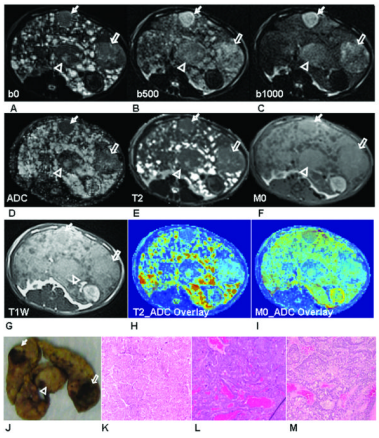

Figure 1.

Three large HCC tumors (HCC-1: arrow head, HCC-2, hollow arrow and HCC-3: solid arrow) were shown in DW-PROPELLER images at b = 0 s/mm^2 (**A**), b = 500 s/mm^2 (**B**) and b = 1000 s/mm^2 (**C**) with resultant ADC map (**D**), PROPELLER T2 map (**E**), M0 map (**F**) and T1W PROPELLER image (**G**). Colored overlays of T2 and M0 maps upon corresponding ADC maps (**H** and **I**) demonstrate the excellent co-registration between these multi-parametric measurements. Qualitatively, tumor positions within these images were well correlated to positions within the sliced liver specimen (**J**). Tissues in each lesion were characterized as HCC in (×400) H&E images (HCC-1 (**K**), HCC-2 (**L**) and HCC-3 (**M**)).

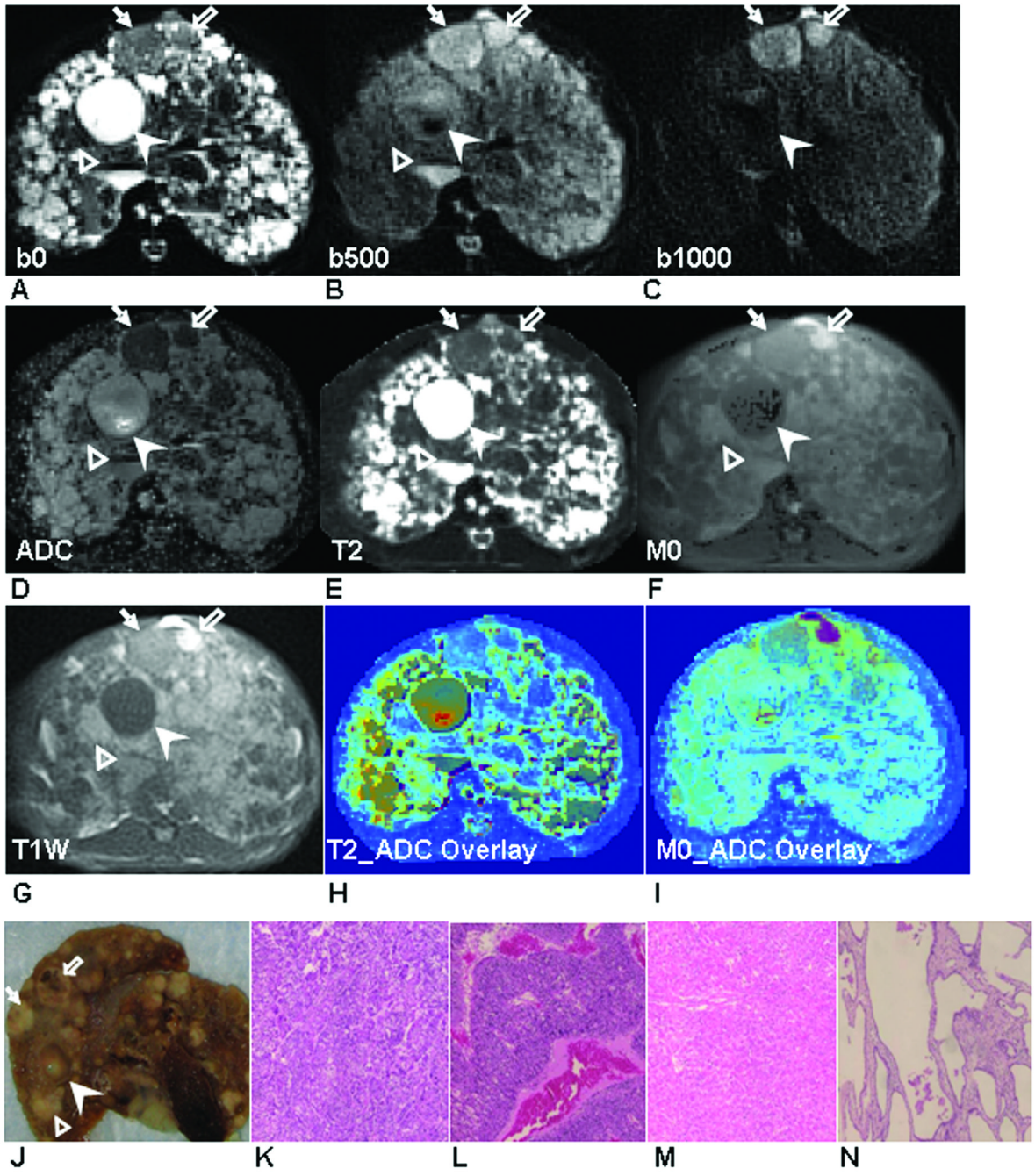

Figure 2.

Two HCC tumors (HCC-1: solid arrow, HCC-2, hollow arrow), one RN (hollow arrow head) and one cyst (solid arrow head) were shown in DW-PROPELLER images at b = 0 s/mm^2 (**A**), b = 500 s/mm^2 (**B**) and b = 1000 s/mm^2 (**C**) with resultant ADC map (**D**), PROPELLER T2 map (**E**), M0 map (**F**) and T1W PROPELLER image (**G**). Colored overlays of T2 and M0 maps upon corresponding ADC maps (**H** and **I**) demonstrate the excellent co-registration between these multi-parametric measurements. Qualitatively, lesion positions within these images were well correlated to positions within the sliced liver specimen (**J**). Tissues in each lesion were characterized as HCC (**K**: HCC-1, **L**: HCC-2), RN (**M**) and cyst (**N**) in (×400) H&E images.

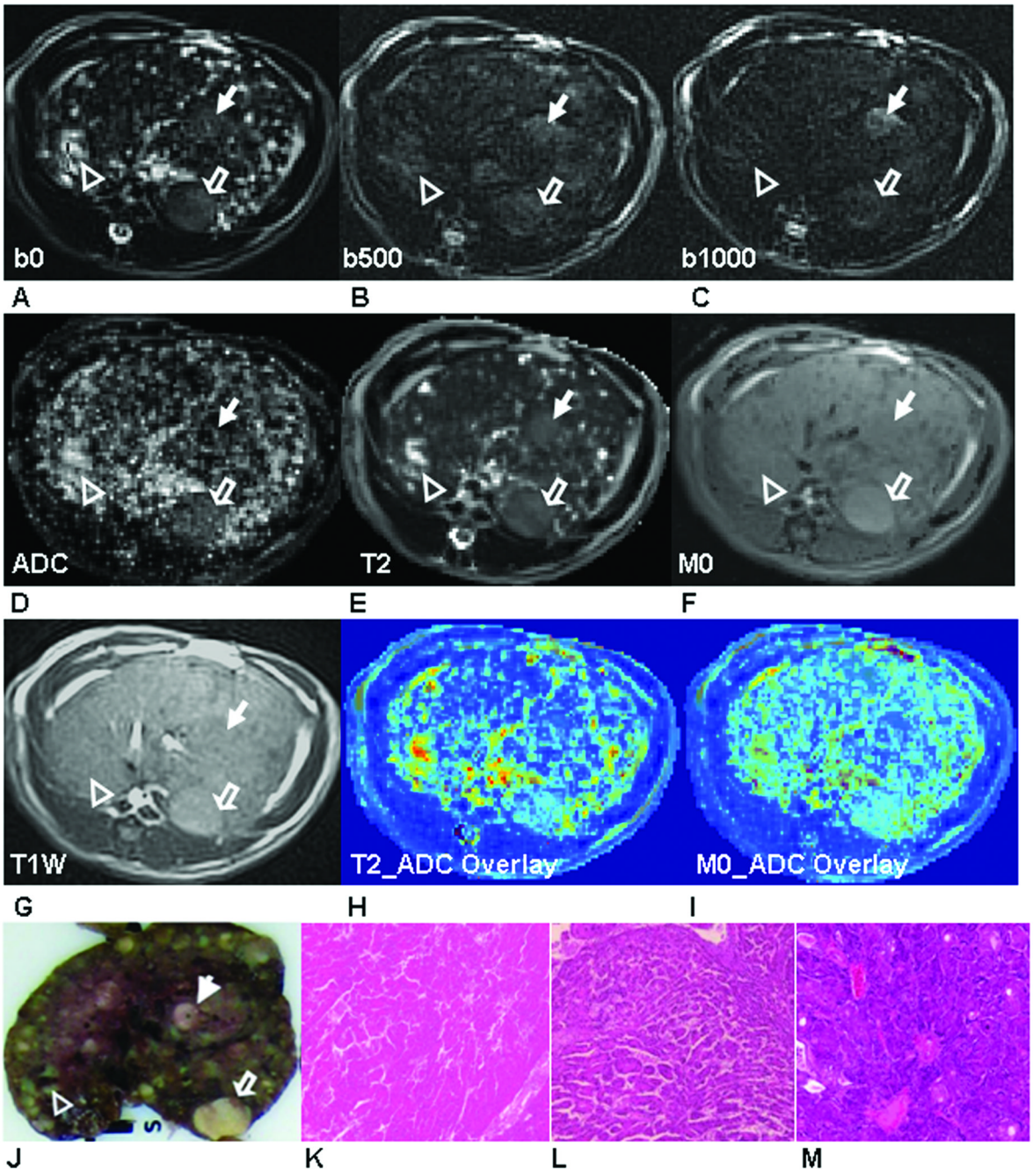

Figure 3.

Two RN (RN-1: solid arrow, RN-2, hollow arrow) and one DN (hollow arrow head) were shown in DW-PROPELLER images at b = 0 s/mm^2 (**A**), b = 500 s/mm^2 (**B**) and b = 1000 s/mm^2 (**C**) with resultant ADC map (**D**), PROPELLER T2 map (**E**), M0 map (**F**) and T1W PROPELLER image (**G**). Colored overlays of T2 and M0 maps upon corresponding ADC maps (**H** and **I**) demonstrate the excellent co-registration between these multi-parametric measurements. Qualitatively, lesion positions within these images were well correlated to positions within the sliced liver specimen (**J**). Tissues in each lesion were characterized as RN (**K**: RN-1 and **L**: RN-2) and DN (**M**) in (×400) H&E images.

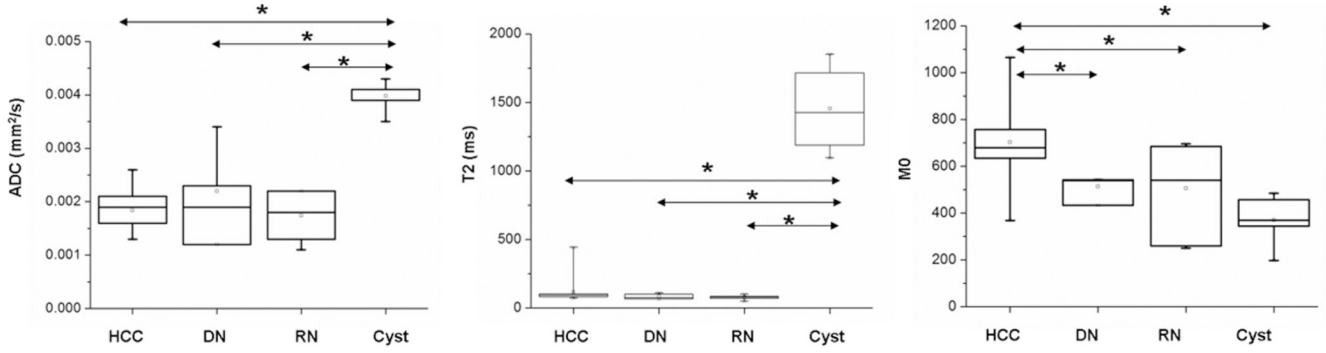

Figure 4.

Box-and-Whisker plots of ADC, T2 and M0 measurements in all hepatic nodules including HCC, DN, RN and cyst, characterized at histopathology. (* denotes a statistically significant difference in independent pair 2-tailed t-test with $p < 0.05$).

Table 1

Hepatic nodule classification using K-means method

K = 4	**I**	**II**	**III**	**IV**
HCC	4	10	3	0
DN	0	2	2	0
RN	0	3	4	0
Cyst	0	0	0	5

K = 5	**I**	**II**	**III**	**IV**	**V**	→		**I**	**II**	**III'**	**IV**
HCC	4	7	2	4	0		**HCC**	4	7	6	0
DN	0	2	1	1	0		**DN**	0	2	2	0
RN	0	3	2	2	0		**RN**	0	3	4	0
Cyst	0	0	0	0	5		**Cyst**	0	0	0	5

K = 6	**I**	**II**	**III**	**IV**	**V**	**VI**	→		**I**	**II**	**III'**	**IV**
HCC	3	9	1	2	2	0		**HCC**	3	9	5	0
DN	0	0	2	1	1	0		**DN**	0	0	4	0
RN	0	2	1	2	2	0		**RN**	0	2	5	0
Cyst	0	0	0	0	0	5		**Cyst**	0	0	0	5

The classified number of each type of hepatic nodules (HCC, DN, RN and cyst) using the multi-dimensional KM classification method (*k* = 4, 5, 6). For k =5 and k = 6, overlapping classes (gray columns) were combined in a new class (III'). Nodule types were determined at histopathology as a reference standard.